Revealing the mid-infrared emission structure of IRAS 16594−4656 and IRAS 07027−7934[1]

D. A. García-Hernández[1,2], A. Manchado[1,3], P. García-Lario[2], A. Benítez Cañete[4], J. A. Acosta-Pulido[1], and A. M. Pérez García[1]

ABSTRACT

TIMMI2 diffraction–limited mid-infrared images of a multipolar proto-planetary nebula IRAS 16594−4656 and a young [WC] elliptical planetary nebula IRAS 07027−7934 are presented. Their dust shells are for the first time resolved (only marginally in the case of IRAS 07027−7934) by applying the Lucy-Richardson deconvolution algorithm to the data, taken under exceptionally good seeing conditions ($\leq 0.5''$). IRAS 16594−4656 exhibits a two-peaked morphology at 8.6, 11.5 and 11.7 μm which is mainly attributed to emission from PAHs. Our observations suggest that the central star is surrounded by a toroidal structure observed edge-on with a radius of $0.4''$ (~ 640 AU at an assumed distance of 1.6 kpc) with its polar axis at P.A.$\sim 80°$, coincident with the orientation defined by only one of the bipolar outflows identified in the HST optical images. We suggest that the material expelled from the central source is currently being collimated in this direction and that the multiple outflow formation has not been coeval. IRAS 07027−7934 shows a bright, marginally extended emission (FWHM=$0.3''$) in the mid-infrared with a slightly elongated shape along the N-S direction, consistent with the morphology detected by HST in the near-infrared. The mid-infrared emission is interpreted as the result of the combined contribution of small, highly ionized PAHs and relatively hot dust continuum. We propose that IRAS 07027−7934 may have recently experienced a thermal pulse (likely at the end of the AGB) which has produced a radical change in the chemistry of its central star.

[1]Instituto de Astrofísica de Canarias, E-38205 La Laguna, Tenerife, Spain; agarcia@iac.es, amt@iac.es, jap@iac.es, apg@iac.es

[2]ISO Data Centre, European Space Astronomy Centre, ESA. Villafranca del Castillo. Apartado de Correos 50727. E-28080 Madrid, Spain; Anibal.Garcia@sciops.esa.int, Pedro.Garcia-Lario@sciops.esa.int

[3]Consejo Superior de Investigaciones Científicas, CSIC

[4]Departamento de Astrofísica, Universidad de La Laguna, E-38205 La Laguna, Tenerife, Spain

Subject headings: stars: AGB and post-AGB — stars: winds, outflows — dust, extinction — planetary nebulae: individual (IRAS 16594-4656, IRAS 07027-7934) — infrared: stars

1. Introduction

Planetary nebulae (PNe) are the result of the evolution of low- to intermediate-mass stars ($0.8–8$ $M_\odot$). These stars experience a phase of extreme mass loss during the previous asymptotic giant branch (AGB) that causes the ejection of the stellar envelope. When this mass loss ceases the AGB phase ends and the star evolves into a short-lived evolutionary stage called the 'post-AGB' or 'proto-PN' (PPN) phase just before the star becomes a PN. At present, the formation of axisymmetric structures in PNe (ranging from elliptical to bipolar) is believed to be completed by the end of the AGB phase (Balick & Frank 2002; Van Winckel 2003). But unlike for PNe, the study of PPNe is more difficult since their central stars (CSs) are usually too cool to photoionize the gas. Therefore, we cannot study the formation of axisymmetric morphologies in PPNe by mapping the ionized gas. We must use alternative techniques based on the analysis of: (i) the light scattered by the surrounding dust at optical wavelenghts; (ii) the neutral molecular gas in the envelope in the near-infrared (H_2), submilimeter (e.g. CO) or radio domain (e.g OH, SiO, H_2O, CO); and (iii) the dust emission emerging at mid- to far-infrared wavelengths.

PPNe generally show a double-peaked spectral energy distribution (SED) (Kwok 1993; Volk & Kwok 1989; van der Veen, Habing & Geballe 1989) with the photospheric emission coming from the central star dominating in the optical range and a strong infrared excess indicating the presence of a cool detached envelope ($T_d\sim150–300$ K). This strong infrared excess is produced by the thermal emission of the dust present in their circumstellar shells previously expelled during the AGB phase. The processes that lead to a wide variety of different morphologies observed in PNe (e.g. Manchado et al. 2000) are, however, still unknown. Several mechanisms have been proposed: the interaction of stellar winds (e.g. Mellema 1993), binary systems as central stars (e.g. Bond & Livio 1990; Morris 1987), non-radial pulsations (e.g. Soker & Harpar 1992) or the influence of magnetic fields (e.g. Pascoli

---

1992; Soker & Harpar 1992; García-Segura et al. 1999). To establish which one(s) of the above is the dominant process, it is essential to study these morphologies as early as possible after the departure from the spherical symmetry takes place, that is, in the PPN phase. Only recently, with the help of high spatial resolution observations it has been possible to study the intrinsic axisymmetric nature of the dust shells around a few compact PPNe at subarcsec level (Meixner et al. 1997; Meixner et al. 1999; Ueta et al. 2001).

In this paper, we present for the first time mid-infrared images (8–13 μm) at subarcsec level of a PPN IRAS 16594$-$4656 (hereafter I16594) and of a very young [WC] PN IRAS 07027$-$7934 (hereafter I07027) with the aim of mapping the dust emission originated in the innermost regions of their circumstellar dust shells. The observations made in the mid-infrared are presented in Sect. 2 while the data reduction process is described in Sect. 3. We show the results obtained in Sect. 4, which are later discussed in Sect. 5. The main conclusions derived from our analysis are given in Sect. 6.

2. Mid-infrared Observations

The observations were carried out on 2001 October 9 and 10, using the imaging mode of TIMMI2 (Reimann et al. 2000; Käufl et al. 2003) attached to the ESO 3.6m telescope (La Silla, Chile). TIMMI2 has an array of 320 $\times$ 240 pixels with a pixel scale of $0.2'' \times 0.2''$ resulting in a field of view of $64'' \times 48''$. The observational conditions were very good (photometric and with a stable seeing of around $0.5''$) and, thus, we could obtain mid-infrared images (at 8.6 μm [N1-filter], 11.5 μm [N11.9-filter] and 11.7 μm [SiC-filter]) of I16594 and I07027 at the diffraction limit of the telescope. The standard nodding/chopping observational technique was used in order to cancel the thermal emission from the atmosphere and from the telescope. An on-chip nodding/chopping throw of 15" along the north-south direction was selected. Due to the short integration times required to avoid saturation in the mid-infrared, each image is a combination of a large number of individual sub-images $\sim$50–100, each one with an integration time between 18 and 40 ms and a chopping frequency around 6 Hz. Total on-source integration times were typically of $\sim$2 minutes. The mid-infrared photometric standard stars HD 29291, HD 156277, HD 196171 and HD 6805 (Doublier et al. 2004) were also observed at different air masses every night to determine the photometric flux conversion from ADUs (Analog to Digital Units) to Jy and to measure the telescope point spread function (PSF).

3. Data Reduction

The data reduction process includes bad pixel correction and the combination of all the images into one single image per filter using standard tasks in IRAF[2]. The flux calibration was made using the conversion factors derived from the observation of standard stars at different air masses. The variation of these conversion factors with air mass was slightly different during the two nights of observation due to the different atmospheric conditions. On October 9 this variation was very small (<10%), so a single averaged conversion factor was used for all the observations performed during the night. However, on October 10 we found larger variations (∼30%). Thus, for I07027 we took the conversion factors derived from the observations of the standard star HD 156277, observed closer in time and at a similar air mass. For each filter the size and morphology of the target stars in our programme was compared with a mean PSF derived from the observation of the standard stars used for the flux calibration. The object name, observing date, filters, central wavelength and width of the different filters used, total on-source integration time, object size, PSF size, integrated and peak fluxes, are listed in Table 1. From the internal consistency of the measurements made on the standard stars we estimate that the photometric uncertainty of our observations is of the order of ∼10%.

The observed PSFs are dominated by diffraction effects. Thus, the Lucy-Richardson deconvolution algorithm as implemented in IRAF (task LUCY) was used in order to recover the actual emission structure of the targets in each filter and remove the effects induced by the telescope PSF, which was found to be very stable. In order to study the goodness of the deconvolution process the standard stars observed for flux calibration purposes were also deconvolved with the same PSF used for the target stars. This exercise is useful to confirm that the deconvolution process does not introduce undesired artifacts. We found that in all cases the deconvolved images of the standard stars spread over only one or two pixels, showing a quasi-point-like brightness distribution. As an example, one of the deconvolved standard stars is shown together with its corresponding raw image in Figure 1.

---

[2]The Image Reduction and Analysis Facility software package (IRAF) is distributed by the National Optical Astronomy Observatories, which is operated by the Association of Universities for Research in Astronomy, Inc., under cooperative agreement with the National Science Foundation

4. Results

4.1. Mid-infrared Morphology of IRAS 16594−4656

Figure 2 shows the raw images of I16594 taken with TIMMI2 (left panel) together with the images obtained after applying the Lucy-Richardson deconvolution algorithm (right panel) above mentioned. The PSFs used for the deconvolution are also shown for comparison. I16594 shows already in the raw images an extended elongated morphology surrounding a complex inner core emission (with a FWHM=1.5" or 3 times the PSF FWHM) which is resolved in more detail after deconvolution. The source center has been determined by averaging the central coordinates of the elliptical isophotes within 20–40% of the peak intensity (this way we avoid any contamination from the core structure). The images displayed in Figure 2 have been centered at this position.

The deconvolved 8.6, 11.5 and 11.7 μm images are shown in the right panel of Figure 2. The overall elliptical shape of the nebula is clear in all three filters with its major axis oriented along the east-west direction (P.A.∼80°) and extends out to at least 3.5″ × 2.1″ at 5% of the peak intensity (10-σ level above the sky background) at 8.6 μm. In addition, a conspicuous double-peaked morphology in the innermost region of the nebulosity is also recovered, suggesting the presence of an equatorial density enhancement (e.g. a dust torus). The two detected peaks are oriented approximately along the north-south direction (P.A.∼−10°) perpendicular to the axis of symmetry defined by the outer elliptical emission. The measured separation between the two peaks is always 0.8″, independent of the filter considered (see Figure 3). In addition, the north-peak (P.A.∼−10°) is about a factor 2 brighter than the south peak (see Figure 3). This finding is not unique to I16594. Indeed, Ueta et al.(2001) found a similar asymmetric profile in IRAS 22272+5435. The origin of this asymmetric appearance of the dust torus is still unclear. Ueta et al. (2001) argued that this can be attributed to asymmetric mass loss and/or an inhomogeneity in the dust distribution. We are confident that the deconvolved structure is real because a very similar emission structure is observed in all three filters. Note that a negligible contribution to the observed flux at 10 μm is expected from the central star of I16594 if this has a B7 spectral type as suggested by Van de Steene, Wood & van Hoof (2000). Hrivnak, Kwok & Su (1999) found that the central star contributes only 3% to the total flux detected in the mid-infrared. We can therefore safely assume that we are just observing the emission structure of the dust in the shell alone. The mid-infrared morphology seen in the deconvolved images is thus interpreted as the evidence of the presence of a dusty toroidal structure with a 0.4″ radius size seen nearly edge-on. Recently, Ueta et al. (2005) based on polarization data also suggest an orientation of the dust torus close to edge-on and they indicate that an inclination angle of roughly 75 ° with respect to the line of sight is derived from a 2-D dust emission model.

This adds I16594 to the short list of PPN where a similar dust torus has been resolved at subarcsec scale.

4.2.   Mid-infrared Morphology of IRAS 07027−7934

The mid-infrared morphology of I07027 is clearly less complex than the one observed in I16594 as deduced already from the raw images shown in Figure 4 (left panel). In this case, only a slightly extended and asymmetric source is detected in the two images available, which correspond to the filters N1 and N11.9 (centered at 8.6 and 11.5 μm, respectively). This can just be due to the larger distance to this source (see Section 5.2.2). Note, that the low level extension to the west of the peak emission seen in both filters seems to be a PSF effect, as it is also observed in the standard stars, although not so prominent.

The deconvolved images of I07027 in the 8.6 and 11.5 μm filters are shown in Figure 4 (right panel). After the deconvolution, a very bright and slightly elongated, marginally extended (FWHM=0.3$''$) emission core is recovered in both filters, oriented along the north-south direction. A similar orientation is observed in recent HST-NICMOS images of I07027 taken in the near-infrared (see Section 5.2). Unfortunately, our TIMMI2 data cannot confirm precisely whether the mid-IR emission peak is exactly coincident with the near-IR emission peak. We propose that the emission core which is detected in the mid-infrared must be coincident with the location of the central star, as the peak emission is observed exactly at the centre of the slight extended emission.

5.   Discussion

5.1.   IRAS 16594−4656

5.1.1.   IRAS 16594−4656 in the literature

I16594 (=GLMP 507) was first identified as a PPN candidate on the basis of its IRAS colors by Volk & Kwok (1989) and van der Veen, Habing & Geballe (1989). It shows a double-peaked spectral energy distribution dominated by a strong mid- to far- infrared dust emission component which is much brighter than the peak in the near-infrared (Van de Steene, van Hoof & Wood 2000). The first indication of the C-rich chemistry of I16594 was the detection of CO molecular emission in its envelope (with $V_{exp}\sim$16 km s^{-1}) by Loup et al. (1990), and the non-detection of OH maser emission (te Lintel Hekkert et al. 1991). More recently, García-Lario et al. (1999) studied the ISO spectrum of this source and confirmed

this classification based on the detection of the characteristic IR emission features generally attributed to PAHs (at 3.3, 6.2, 7.7, 8.6 and 11.3 μm) together with relatively strong features at 12.6 and 13.4 μm which indicates a high degree of hydrogenation in these PAHs. The ISO spectrum also reveals the presence of strong 21, 26 and 30 μm dust emission features (see Figure 5), adding I16594 to a short list of known PPNe displaying this set of still unidentified features.

The optical spectrum of I16594 shows only the hydrogen Balmer emission lines over an extremely reddened stellar continuum (E_{B-V}=1.8, Van de Steene & van Hoof 2003) consistent with a B7 spectral type if dereddened. HST optical images show the presence of a bright central star surrounded by a multiple-axis bipolar nebulosity (seen in scattered light) with a complex morphology at some intermediate viewing angle (see Figure 6). The size of this optical nebulosity is 6.3″ × 3.3″ at $3\sigma_{sky}$ level (Hrivnak, Kwok & Su 1999).

In the literature there are several indications of the presence of a circumstellar disc or a torus (an equatorial density enhancement) around I16594. The highly collimated structure seen in the HST optical images and the non-detected radio-continuum emission ($<10~mJy$) by Van de Steene & Pottasch (1993) suggest that the emission lines observed in the optical spectrum are the result of shock excitation produced by a fast bipolar wind from the central source in interaction with the slow AGB wind. In agreement with this hypothesis García-Hernández et al. (2002) reported the detection of H_2 shock-excited emission in I16594, later confirmed by Van de Steene & van Hoof (2003) through a more detailed analysis of the H_2 spectrum. They postulate that the H_2 emission originates mainly where the stellar wind is funnelled through a circumstellar disc or torus. More recently, Hrivnak, Kelly & Su (2004) presented HST-NICMOS near-infrared images of I16594 which show that this emission is originated in regions where shocks must be taking place. Polarization measurements originally taken by Su et al. (2003) and later analyzed by Ueta et al. (2005), who presented a PSF subtracted map of the polarized light, suggest the presence of an equatorial enhancement in I16594 as well. However, Van de Steene, van Hoof & Wood (2000) failed to detect any extended emission in their N-band TIMMI images of I16594 in a previous attempt to search for mid-infrared emission coming from this torus, but they observed the source with a lower spatial resolution (pixel scale of 0.66″), and under poor weather conditions.

5.1.2. A Dusty Toroidal Structure around IRAS 16594−4656

There exists more than a dozen PPN shells that have been resolved in the mid-infrared so far. However, only a few of them show some structure at mid-infrared wavelengths. Meixner et al. (1999) found two different classes of mid-infrared morphologies. They distinguish

those sources with a mid-infrared core/elliptical structure from those with a toroidal one and they argue that this morphological dichotomy is due to a difference in optical depth. In their sample there are only 4 out of 6 toroidal PPN/PNe in which the central dust torus is well resolved in two emission peaks. This work adds I16594 to this short list. In Table 2 we list the few known toroidal PPN/PNe sample together with some of their main observational characteristics, such as the spectral type of the central star, C/O ratio, evolutionary classification, optical morphology, and the list of mid-infrared dust emission features detected.

An inspection of Table 2 clearly indicates that I16594 is now a toroidal-PPN with the earliest spectral type known. The other PPNe with mid-infrared toroidal structures have all F-G spectral types, while IRAS 21282+5050 is already a young PN with an O9-type central star. It seems that many of these sources show a C-rich chemistry (indicated by the presence of PAH emission features) but the number of objects considered is still small and the statistics are very poor. It is interesting to remark the fact that all mid-infrared toroidal-PPN/PNe have bipolar/multipolar optical morphologies where the central star is clearly seen. In contrast, the central star is rarely seen in the mid-infrared core/elliptical class sources described by Meixner et al. (1999) and almost all of them display bipolar morphologies in the optical. In addition, the mid-infrared core/elliptical sources are typically O-rich and show deep silicate absorption features at 9.8 μm in their mid-infrared spectra, indicating that they may be optically thick at mid-infrared wavelengths (Meixner et al. 1999). The different optical morphology (with or without a visible central star) and the apparent differences in dust properties (optical thickness in the mid-infrared) suggest that mid-infrared toroidal PPNe might be surrounded by a dust torus which is optically thin at mid-infrared wavelengths and, thus, not able to obscure the central star in the optical domain, while, in contrast, mid-infrared core/elliptical PPNe would be surrounded by an optically thick dust torus/disk which would completely obscure the central star in the optical (Meixner et al. 1999, 2002; Ueta et al. 2000, 2003).

Our deconvolved mid-infrared images of I16594, of much better quality than those previously reported by Van de Steene, van Hoof & Wood (2000), reveal directly for the first time the presence of an optically thin dusty toroidal structure with a radius of 0.4″. Unfortunately, the distance determinations to I16594 are quite uncertain and, thus, a direct transformation of this observed size into an absolute physical value is not straightforward. Estimations based on the observed reddening are hampered by the fact that the overall extinction is always a combination of interstellar and circumstellar reddening. And in the case of I16594 there seems to be a considerable contribution from the circumstellar component. Calculations made by Van de Steene & van Hoof (2003) based on the intrinsic colors expected for a B7 central star in the optical and in the near-infrared suggest a total extinction of A_V=7.5 mag

with R_V=4.2. With this value for the extinction and the flux calibration from the Kurucz model a distance of (2.2±0.4) $L_4^{1/2}$ kpc is obtained, where L_4 is in units of 10^4 $L_\odot$. We have tried to derive our own distance estimate to I16594 based on the analysis of the overall SED, from the optical to the far-infrared. For this we put together the IRAS fluxes at 12, 25, 60 and 100 μm, the near-infrared JHKL magnitudes from García-Lario et al. (1997) and the BVRI magnitudes from Hrivnak, Kwok, & Su (1999). The observed BVRI and JHKL fluxes were corrected for extinction using the total extinction of A_V=7.5 mag determined by Van de Steene & van Hoof (2003) and the extinction law from Cardelli, Clayton & Mathis (1989). Then, a distance-dependent luminosity was obtained by integrating the observed flux at all wavelengths and extrapolating the IRAS fluxes to the infinite following Myers et al. (1987). This way, a distance of 2.1 $L_4^{1/2}$ kpc is obtained, in very good agreement with the previous determination by Van de Steene & van Hoof (2003). Assuming a luminosity of 6,000 $L_\odot$, which is the theoretical luminosity expected for a post-AGB star with a core mass of 0.60 $M_\odot$ (Schönberner 1987), a distance of 1.6 kpc to I16594 is derived, value that will be adopted in the following discussion. The value of 0.60 $M_\odot$ is chosen for the mass of the core because the mass distribution of planetary nebulae central stars is strongly peaked at this value (Stasynska, Gorny & Tylenda 1997).

At a distance of 1.6 kpc, the extended emission detected in our deconvolved mid-infrared images of I16594 would correspond to a dusty toroidal structure with a radius of $\sim$640 AU. Assuming that the CO emission detected towards I16594 is a good tracer of the dusty torus structure and considering the CO expansion velocity of 16 km s^{-1} measured by Loup et al. (1990), a dynamical age of the dusty torus structure of $\sim$190 yr can be estimated. This dynamical age is quite consistent with a source which has left the AGB very recently.

5.1.3. Dust Temperature

The radiation transfer equation in the interior of a dust cloud adopts a simple form when the energy source is a single exciting star under the optically thin approximation and assuming thermal equilibrium. Under these conditions, the mean color temperature of the dust can be obtained from a simple equation (see e.g. Evans 1980) which relates the measured fluxes $S_{\nu 1,2}$ at two different wavelenghts $\lambda_{1,2}$ and the dust emissivity index (which depends on the assumed dust model), assuming a homogeneous dust distribution throughout the cloud. It should be noted that the assumption of the central star as the only source of energy for dust heating is appropiate for I16594 because direct stellar ratiation is the dominant heating source for the circumstellar dust grains in the shell. In particular, we have investigated whether dust heating due to line emission could also contribute to the observed emission

and found that this effect is negligible, as the value of the Infrared Excess(IRE) for I16594, defined as the ratio between the observed total far infrared flux and the expected far infrared flux due to absorption by dust of Ly α photons (see e.g. Zijlstra et al.1989), is ~ 400.

In principle, one could construct color temperature maps for the dust from the analysis of the 8.6 and 11.5 μm TIMMI2 images of any given source, as long as these bands are representative of the dust continuum emission. Unfortunately, in the case of I16594, the 8.6 and 11.5 μm emission is strongly affected by the PAH emission features which are clearly visible in the ISO spectrum (see Figure 5). Thus, the temperature values derived this way are not expected to represent realistic estimations of any physical temperature in the shell. The same problem is found if we try to derive the dust temperature from the IRAS photometry at 12 and 25 μm, since both filters are also strongly affected by the presence of dust features, as ISO spectroscopy reveals. This is confirmed by the strongly different mean dust temperatures $T_{8.6/11.5}$ of 227 K and $T_{12/25}$ of 129 K, derived (assuming a dust emissivity index of 1) from our mid-infrared data and from the IRAS photometry at 12 and 25 μm, respectively.

A more reliable dust temperature can be directly estimated from the observed size of $0.4''$ for the inner radius of the dusty torus assuming that this is the equilibrium radius for the bulk of the dust emitting at mid-infrared wavelengths. Based on the formula worked out by Scoville & Kwan (1976), this can be calculated using the equation:

$$T_d = 1.64 f^{-1/5} r_{eq}^{-2/5} L_*^{1/5} \tag{1}$$

where T_d is the dust temperature in K, f is the emissivity of the dust, r_{eq} is the equilibrium radius in pc, and L_* is the source luminosity in $L_\odot$.

We decided to use for our calculations a basic dust model composed by hydrogenated amorphous carbon grains (HACs; type BE of Colangeli et al. 1995), whose emissivity index is $\sim$1. The selection of this dust model to reproduce the dust continuum emission observed in I16594 is justified by the presence of highly hydrogenated PAHs in the ISO spectrum (García-Lario et al. 1999). In order to calculate the dust emissivity, the mass extinction coefficient value for hydrogenated amorphous carbon was taken from appendix A of Colangeli et al. (1995) at the central wavelength between the two filters. Then, a typical grain density of 1.81 g cm^{-3} (Koike, Hasegawa & Manabe 1980) was assumed. Finally, this quantity was multiplied by a dust grain size in the range 0.001-0.1 μm obtaining a dust emissivity f. Note that a dust grain size of 0.01 μm is a reasonable mid-range size for circumstellar carbon dust (e.g. Jura, Balm & Kahane 1995). The dust temperature in thermal equilibrium at $0.4''$ (or $\sim$640 AU at the assumed distance of 1.6 kpc) can then be derived using the dust emissivity f and the assumed luminosity of the source (6,000 L$_\odot$). This way, a dust temperature T_d=237 K is found for a mid-range dust grain size of 0.01 μm. A smaller or a larger dust grain size of 0.001 and 0.1 μm would imply dust temperatures of 376 and 150 K, respectively.

We are conscious that the assumption of spherical geometry may not be valid for the circumstellar envelope of I16594 where the emission is clearly asymmetric and the geometry assumes a toroidal shape, according to our mid-IR images. Note that adopting a more complex, axysimmetric geometry would esentially translate into grains being more effectively heated in the biconical opening angle defined by the dust torus because of the different local optical depth. In spite of this, our simple model can be used irrespective of the shell geometry when applied to dust grains at the inner radius of the shell. The use of more detailed axysimmetric, multiple grain size models is beyond the scope of this paper. In addition, the presence of a dust torus close to the star with respect the spherical case mainly influences the optical and near-infrared radiation. A large effect on the mid- to far-IR emission is not expected (see e.g. Ueta & Meixner 2003). In this sense, spatially unresolved SEDs do not provide any spatial information necessary to constrain the geometry and inclination angle of the PPN dusty shells.

5.1.4. Comparison with ISO data

Another dust temperature estimate can be derived by fitting one (or more) blackbodies to the available ISO data by considering fluxes representative of the underlying continuum at carefully selected wavelengths not affected by any dust feature. We did this by selecting the ISO fluxes at 6.0, 9.4, 14.3, 18.0, and 45.0 μm plus the IRAS fluxes at 60 and 100 μm. The best fit to the overall SED is obtained with a combination of two blackbodies (with an emissivity index of 1) with temperatures of 273 K and 130 K, respectively, as we can see in Figure 5, where we display the SED of I16594 from 1 to 100 microns together with the two blackbodies. We find that actually the warm component (at 273 K) dominates in the wavelength range of the N1-filter (at 8.6 μm) while the cool component (at 130 K) dominates in the N11.9-filter range (at 11.5 μm). Overimposed on the continuum emission, strong PAH features are also clearly contributing to the observed emission. Note that the PAH emission features observed at the ISO short wavelengths as well as the dust features at 21, 26 and 30 μm, the latter extending from 20 to 40 μm, are intentionally excluded from the fitting because they are not representative of the dust continuum emission. In particular, the 30 μm feature overlaps with the 26 μm feature, and even with the 21 μm feature and the continuum level is well below the flux detected by ISO at 22–24 microns (see e.g. the analysis of the similar sources IRAS 20000+3239 and HD 56126 shown in Fig. 10 of Hony, Waters & Tielens 2002). At present, most of these features remain still unidentified, although several possible carriers have been proposed in the literature, e.g. fullerenes, TiC, SiC for the 21 μm feature (García-Lario et al. 1999; von Helden et al. 2000; Speck & Hofmeister 2003); MgS for the broad 30 μm feature (Hony, Waters, & Tielens 2002 and references therein).

Using the above two dust temperatures we can estimate the size of the dust grains which are expected to emit in equilibrium at the distance of $0.4''$ from the central star which is derived from our mid-IR images. This is found to correspond to small dust grains with a size of $0.005\ \mu$m in the case of the warm dust component emitting at 273 K which dominates at $8.6\ \mu$m (comparable to the typical size of small PAH clusters). Dust grains with the same size emitting at 130 K (note that this cold dust emission dominates at 11.5 and $11.7\ \mu$m) would need to be located at $\sim$4075 AU from the central star, which corresponds to a projected $\sim$2.5$''$ on the sky at the assumed distance. This is considerably beyond the observed extension of the inner shell in the mid-infrared. A surface brightness of $\sim$350 mJy/pixel can be roughly estimated for the continuum emission expected under these conditions, well above ($\sim$50-σ) our detection limit. The fact that we do not detect this extended emission in our images suggests that the angular size of the region giving rise to the bulk of the hot dust emission is much smaller than that of the region emitting at 130 K. Note that, assuming e.g. that the cold dust emission extends homogeneously over the larger aperture used by ISO, we find that the surface brightness would be just below the 3-σ level of the sky background and, as such, undetectable in our TIMMI2 images. The similar extension and morphology of the mid-infrared emission observed at 8.6, 11.5 and $11.7\ \mu$m suggests that the contribution from PAHs observed in the ISO spectrum must be dominant in our TIMMI2 images, and that these PAHs may be well mixed with the small, hot dust grains responsible for the underlying continuum, being mainly distributed along the torus.

Considering the information available and the limited spectral coverage, an alternative scenario which cannot be ruled out completely might be that both small, hot dust grains and large, cold dust grains could be co-located in the dust torus. This would be possible if a larger grain size ($\geq$0.1 μm) is assumed for the cold dust. Note that, in a non-spherical (torus) distribution of the dust, the shielding can become very efficient and the density very high in the outer equatorial regions, where the dust can grow and get colder, protected both from the radiation from central star and from the ISM UV radiation field. This would explain the larger size of the cold dust grains in the torus. In contrast, small, hot dust grains are expected to dominate in the inner boundary of the torus. Unfortunately, the spatial resolution of our images is not enough to resolve the grain size distribution within the torus.

5.1.5. Collimated outflows in IRAS 16594−4656

I16594 has also been observed by the HST in the optical, through the broad F606W continuum filter with the Wide Field Planetary Camera (WFPC2) under proposal 6565 (P.I.: Sun Kwok), and in the near-infrared, through the narrow F212N (H_2) and F215N (H_2-

continuum) filters with the Near Infrared Camera and Multi Object Spectrometer (NICMOS) under proposal 9366 (P.I.: Bruce Hrivnak). In the optical, I16594 shows a flower-shaped morphology where several petals (or bipolar lobes) can be identified at the opposite sides of the central star with different orientations, which has been suggested to be a result of episodic mass ejection (Hrivnak, Kwok, & Su 1999). Similar structures have also been detected in other PPNe (e.g. Hen 3-1475; Riera et al. 2003) and in more evolved PNe (e.g. NGC 6881; Guerrero & Manchado 1998) and they have been interpreted as the result of episodic mass loss from a precessing central source (e.g. García-Segura & López 2000). From the HST optical images (taken from the HST Data Archive) we identify pairs of elongated structures with at least four different bipolar axes at P.A.$\sim$34°, $\sim$54°, $\sim$84° and $\sim$124°.

In Figure 6 we have displayed the contour map of the deconvolved mid-infrared images of I16594 obtained with TIMMI2 in the N1 and N11.9 filters overlaid on the optical HST-WFPC2 image taken in the F606W filter. Remarkably, we can see that the axis of symmetry defined by the mid-infrared emission nicely coincides with only one of the bipolar axes that can be identified in the optical images, in particular with that oriented at P.A.$\sim$84°. If this emission is a good tracer of the hot dust in the envelope and we accept that this hot dust must have been recently ejected from the central star we can interpret the observed spatial distribution in the mid-infrared as the result of the preferential collimation of the outflow material along this direction in the most recent past.

Remarkably, the H_2 shocked emission detected with HST-NICMOS in the near-infrared is also found mainly distributed following the same bipolar axis (Hrivnak, Kelly & Su 2004) and nicely coincides with the mid-IR emission seen in our TIMMI2 images. This is shown in Figure 7, where the H_2 continuum-subtracted HST-NICMOS image is shown together with a contour map of the deconvolved mid-infrared image taken in the N11.9 filter. Note that the H_2 image (at 2.122 μm) showed in Figure 7 was continuum-subtracted using the HST-NICMOS image taken in the adjacent continuum at 2.15 μm (both images were also taken from the HST Data Archive). Interestingly, we found that the H_2 emission is mainly coming from the walls of the bipolar lobe oriented at P.A.$\sim$84° identified in the HST optical images. In addition, four additional clumps of much weaker H_2 emission are detected at the end of each of the other two point-symmetric outflows associated to I16594 (Hrivnak, Kelly & Su 2004). The stronger emission detected along the walls of this bipolar lobe suggests that the interaction of the fast wind from the central star with the slowly moving AGB wind is currently taking place preferentially also along this axis of symmetry. This suggests that the formation of the multiple outflows observed in I16594 has not been simultaneous. The rest of bipolar outflows observed at other orientations in the optical images taken with HST must then be interpreted as the result of past episodic mass loss ejections. As such, they must contain much cooler dust grains which are then only detectable in the optical because

of their scattering properties.

5.2.   IRAS 07027−7934

5.2.1.   IRAS 07027−7934 in the literature

I07027 (=GLMP 170) is a very peculiar young PN. It has a central star that was classified by Menzies & Wolstencroft (1990) as of [WC11]-type. At present, there are only about half a dozen PNe with a central star classified as [WC11]. They all have stellar temperatures between ∼28,000 and 35,000 K (Leuenhagen & Hamann 1998) and are supposed to be in the earliest observable phase of its PN evolution, soon after the onset of the ionization in their circumstellar envelopes. I07027 is also among the brightest IRAS PNe and it has IRAS colors similar to other young PNe (Zijlstra 2001). The youth of I07027 as a PN is also evidenced by the detection of OH maser emission at 1612 MHz (Zijlstra et al. 1991), which is usually observed in their precursors, the OH/IR stars, but very rarely in PNe. The OH emission is single-peaked, which is interpreted as being detected only coming from the blue side of the shell, as the consequence of the ionized inner region being optically thick at 1612 MHz. This is supported by the shift in velocity with respect to the CO emission, which has also been detected toward this source, and from which an expansion velocity of 14.5 km s^{-1} is derived (Zijlstra et al. 1991).

The detection of strong PAH features and crystalline silicates in the ISO spectrum (Cohen et al. 2002; Peeters et al. 2002) indicates the simultaneous presence of oxygen and carbon-rich dust in the envelope. Remarkably, all other [WC] CSPNe observed with ISO show a mixed chemistry as well (Cohen et al. 2002) but I07027 is the only known [WC] star belonging to the rare group of PNe with OH maser emission, and therefore it links OH/IR stars with carbon-rich PNe.

Zijlstra et al. (1991) published an Hα image of I07027 taken with the ESO 3.5m NTT telescope. This image shows a stellar core with non-gaussian wings extending to a maximum diameter of about 15″, which may be mostly due to light scattered by neutral material and dust grains in the envelope. García-Hernández et al. (2002) detected H$_2$ fluorescence-excited emission from this source, in agreement with the round/elliptical Hα morphology of the nebula and the temperature of the central star.

I07027 had never been imaged in the mid-infrared before. Thus, our observations are the first attempt to reveal the spatial distribution of the warm dust in this peculiar object.

5.2.2. The Marginally Extended Mid-infrared Core of IRAS 07027–7934

The deconvolved mid-infrared images of I07027 displayed in Figure 4 show a slightly extended emission at 8.6 and 11.5 μm. This mid-infrared emission is only marginally resolved (with a FWHM=0.3″ as compared to the typical PSF size of FWHM≤0.2″ measured in the deconvolved standard stars) and is elongated along the north-south direction. Zijlstra et al. (1991) predicted for this source a radio flux density of 10 mJy assuming E_{B-V}=1.1 and T_e=10^4 K. In addition, by using a plausible radio brightness temperature of 10^3 K they predicted an angular diameter of ∼0.3″ for the ionized region. This size for the ionized region is consistent with the measured size of the bright mid-infrared core seen in our deconvolved images of I07027.

Unfortunately, there are no HST images of I07027 available in the optical but it has very recently been observed in the near-infrared through the broad F110W (J-band) and F160W (H-band) continuum filters with NICMOS under proposal 9861 (P.I.: Raghvendra Sahai). In Figure 8 we have displayed the still unpublished near-infrared HST images of I07027 (taken from the HST Data Archive) together with the contour levels of the deconvolved mid-infrared image taken by us in the N11.9 filter. In the F160W filter, I07027 shows a bright extended core (with FWHM=0.25″), which is slightly elongated along the north-south direction, in agreement with the mid-infrared structure seen in our deconvolved TIMMI2 images. This core is surrounded by a fainter elliptical nebulosity extended along the NW-SE direction with a total size of ∼1.6″ × 2.1″ at 1% of the peak intensity. The HST image in the F110W filter shows a slightly less extended emission of ∼1.1″ × 1.5″ (at 1% of the peak intensity) and shows a very similar morphology. In this case, a central point source is clearly detected which corresponds very probably to the central star, which is barely detected in the F160W image.

Similarly to what we did for I16594 we have also estimated the distance to I07027. In this case we constructed the SED of I07027 by combining the available IRAS fluxes at 12, 25, 60 and 100 μm with the JHKL and BVRI photometry taken from García-Lario et al. (1997) and Zijlstra et al. (1991), respectively. The observed fluxes were also corrected for reddening adopting the extinction law from Cardelli, Clayton & Mathis (1989) and the value of E_{B-V}=1.1 derived by Zijlstra et al. (1991) through the measurement of nearby stars, with R_V=3.1. Then, a distance of 4.1 $L_4^{1/2}$ kpc is obtained. Note that I07027 is located at a much higher galactic latitude (b=−26°) than I16594 (b=−3°) and at such high galactic latitudes so much interestellar reddening is unexpected. Thus, we interpret that the observed reddening E_{B-V}=1.1 is mainly circumstellar in origin. On the other hand, most of the flux is emitted in the infrared where the effect of the interstellar/circumstellar extinction is mild. This is probably the reason why a very similar luminosity of 4.2 $L_4^{1/2}$ kpc was obtained by

Surendiranath (2002), who derived this value by integrating the photometric fluxes from 0.36 μm to 100 μm, but without introducing any correction for extinction. Assuming a standard luminosity of 6,000 L$_\odot$ for I07027, a distance of 3.2 kpc is derived, in agreement with the distance of 3–5 kpc suggested by Zilstra et al. (1991). At this distance, the core size would correspond to ∼960 AU.

5.2.3. Dust Temperature

As for I16594, stellar light must be the dominant heating source for the circumstellar dust grains in I07027. This is confirmed by Zijlstra et al. (1991), who derived an Infrared Excess (IRE) of 93 for this source, indicating that dust heating by line emission can also be neglected in I07027. Again, we cannot interpret our mid-infrared observations of I07027 in terms of dust temperatures in the shell because the ISO spectrum of I07027 (Cohen et al. 2002) shows that the 8.6 and 11.5 μm filters are also heavily affected by strong PAH emission features. In particular, the PAH emission features around 8 μm (at ∼7.7 and 8.6 μm) are much stronger in this case than the feature located at 11.3 μm. Thus, the dust temperature values derived would be unrealistically high. Using IRAS data and assuming a dust emissivity index of 1, a mean dust temperature $T_{12/25}$ of 148 K is derived, while the TIMMI2 data gives a $T_{8.6/11.5}$ of ∼363 K. The strong differences in the derived temperatures confirm that the PAH emission is dominating the emission observed in the mid-infrared.

In contrast to I16594, the ISO spectrum of I07027 shows much weaker emission features at 12.6 and 13.4 μm, which are the signatures of the CH out-of-plane bending vibrations for hydrogens in positions duo and trio, respectively (Pauzat, Talbit & Ellinger 1997) and indicate that the PAH population in I07027 is largely dehydrogenated. Then, for the modelling of the dust emitting at mid-IR wavelengths we made the same assumptions as in the case of I16594 (see Section 5.1.3) but this time we adopted a composition dominated by dehydrogenated amorphous carbon grains (type ACAR of Colangeli et al. 1995). Under these assumptions and taking into account the dust equilibrium radius to be consistent with the 0.3″ (or ∼960 AU at the assumed distance of 3.2 kpc) of the shell (which is the radius at ∼90% of the peak intensity) seen in our mid-infrared deconvolved images we obtain a dust temperature of 219 K for a mid-range dust grain size of 0.01 μm. For a larger dust grain size of 0.1 μm a smaller dust temperature of 138 K is derived while a smaller dust grain size of 0.001 μm yields a dust temperature of 347 K. Note that if the dust grains were located closer to the central star than the 0.3″ derived from our mid-infrared images, the dust temperatures above derived should then be considered as lower limits.

5.2.4.   Comparison with ISO data

The validity of the range of possible dust temperatures derived from our TIMMI2 observations can be further explored by looking at the ISO spectrum originally published by Cohen et al. (2002). In a similar way as we did for I16594, the SED can be fitted by a two-component dust continuum with temperatures of T_{BB1}=430 K and T_{BB2}=110 K, respectively. The warm component in this case completely dominates in the wavelength range of our TIMMI2 observations (where also strong PAH features are found) while the cool component dominates at longer wavelengths, where crystalline silicate dust features are also detected on top of the continuum emission.

By forcing the dust equilibrium radius to be consistent with the 0.3″ seen in our mid-IR deconvolved images, we need to assume in this case a very small grain size of <0.001 μm in order to reproduce the dust temperature of 430 K derived from the ISO spectrum. This suggests that the mid-infrared emission at ∼430 K must be the result of the combined contribution of small PAH molecules, located very close to the central star, and relatively hot dust continuum. In this case, the PAH population must be subject to a relatively strong UV field, consistent with the narrow features detected by ISO (in contrast to the broader features observed in I16594). Actually, the ISO spectrum of I07027 shows that the PAH emission features at 3.3 and 11.3 μm are weak compared with the emission features located at 6.2, 7.7, and 8.6 μm, which is also indicating a high degree of ionization in the population of PAHs (see Figure 2 in Allamandola, Hudgins & Sandford 1999). Note, however, that if the UV radiation field becomes too strong the PAH molecules can be destroyed, especially the small ones with a size ∼20−30 carbon atoms (see e.g. Allain, Leach & Sedlmayr 1996). This means that the C-rich dust seen in the ISO spectrum subject to the UV irradiation coming from the central star must be shielded from the stronger ISM UV radiation field by the outer layers of the circumstellar shell, where the OH maser emission is originated.

For the cool dust emitting at 110 K, a different dust model was assumed, composed mainly of astronomical silicates. This choice takes into account the O-rich nature of the crystalline silicates detected in the ISO spectrum at wavelengths longer than 25 μm. The crystalline silicates are expected to be formed in the circumstellar dust shells of evolved stars at temperatures in the range 60−160 K (Molster et al. 2002b). The mean emissivity value adopted between 25 and 60 μm was taken from Figure 5 in Draine & Lee (1984). If we try to confine this cool O-rich dust to the observed extension of 0.3 ″ we would need to adopt a very large dust grain size of >0.1 μm. Note that for this O-rich cool component we derive dust equilibrium radii of ∼0.02, ∼0.05 and 0.17 pc (or 1.1″, 3.4″ and 10.4″ at 3.2 kpc) for dust grain sizes of 0.1, 0.01 and 0.001 μm, respectively, which in all cases are inconsistent with our mid-infrared observations. These calculations indicate that independent of the dust grain

size considered, the O-rich cool dust must be located much farther away from the central source than the C-rich warm dust emission (at 430 K) detected in the mid-infrared This different relative distribution of O-rich and C-rich dust would also be consistent with the detection of OH maser emission from the outer shell and suggests that the material expelled by the central star during the previous AGB phase was predominantly O-rich.

5.2.5. Evolutionary Status of IRAS 07027−7934

At present, the evolutionary status of I07027 is not well understood. The hydrogen-deficiency of the central star together with the mixed dust chemistry (C-rich and O-rich) is a common finding among the limited sample of known [WC] PNe (De Marco & Soker 2002; Cohen et al. 2002). The most promising scenarios to explain the current observational properties of this rare class of PNe are: (i) the so-called 'disk-storage' scenario (Jura, Chen & Plavchan 2002; Yamamura et al. 2000); (ii) a final thermal pulse while the star was still in the AGB; or (iii) a late thermal pulse during the post-AGB evolution (Herwig et al. 1997, 1999; Herwig 2000, 2001; Blöcker 2001).

The disk-storage scenario invokes the presence of a binary system in which the O-rich silicates are trapped in a disk formed by a past mass transfer event, with the C-rich particles being more widely distributed in the nebula as a result of recent ejections of C-rich material. This type of dusty disk structures have been detected in some PPN/PNe with binary [WC] central stars like CPD−56°8032 (De Marco, Barlow & Cohen 2002) or in the Red Rectangle (HD 44179) (Waters et al. 1998), but no firm evidence of the presence of any disk-like structure nor of the binarity of I07027 exists yet.

Both a final thermal pulse in the AGB and a late thermal pulse during the post-AGB phase can eventually produce a sudden switch to a C-rich chemistry and a strong stellar wind, which is also characteristic of these [WC] CSPNe. However, because of the short lifetime of stars in the post-AGB phase, the latter is expected to be a rare phenomenon. Models predict that post-AGB stars which experience a late thermal pulse evolve back into the AGB (the so-called "born-again" scenario, e.g., Herwig 2001; Blöcker 2001). As a result of this, they show a fast spectroscopic evolution in the H-R diagram as well as peculiar spectroscopic features (e.g., Asplund et al. 1999; Lechner & Kimeswenger 2004; Hajduk et al. 2005) which are not observed in I07027, nor in any other known [WC] CSPNe.

A final thermal pulse in the AGB phase seems to be a more plausible explanation since it does not require the assumption of exotic scenarios. As we have discussed in Section 5.2.4, the emission detected in our mid-infrared images can be mainly attributed to ionized PAHs

plus thermal emission from relatively warm dust ($\sim$430 K) located very close to the central source. The OH maser emission detected by Zijlstra et al. (1991) supports the idea that the envelope of I07027 was until very recently O-rich. It is very difficult to explain how a low-mass disk around a binary system, which could act as an oxygen-rich reservoir, may be able to sustain such a luminous maser emission. Attending to geometry considerations, Zijlstra et al. (1991) suggests that the star must have changed its chemistry within the last 500 yrs. I07027 may have experienced a final thermal pulse in the AGB which has produced the recent switch to a C-rich chemistry. All C-rich material would then be warm as a consequence of its very recent formation and, thus, located very close to the central source (as it is actually observed) while the cooler O-rich material ejected during the previous AGB phase is then found now only farther away from the central source.

In contrast, the typical disk sources with dual chemistry which are known to be binary systems show a completely different relative distribution of O-rich and C-rich dust. Waters et al. (1998) found that the PAH emission at 11.3 μm has a clumpy nature and comes from the extended nebula around HD 44179, while the O-rich material is located in a circumbinary disk. More recently, the bipolar post-AGB star IRAS 16279$-$4757 has been studied in the mid-infrared by Matsuura et al. (2004). They found that the PAH emission is enhanced at the outflow, while the continuum emission is located towards the center. Thus, they suggest the presence of a dense O-rich torus around an inner, low density C-rich region and a C-rich bipolar outflow resembling the morphology attributed to HD 44179. The observational characteristics of I07027 indicate a totally different formation mechanism, which are only consistent with a very recent change of chemistry from O-rich to C-rich.

6. Conclusions

We have presented diffraction limited mid-infrared images of the PPN I16594 and the [WC] PN I07027 at 8.6, 11.5 and 11.7 μm taken under exceptionally good seeing conditions ($\leq$0.5$''$). By applying the Lucy-Richardson deconvolution algorithm, we have resolved, for the first time, the subarcsecond dust shell structures around both objects.

I16594 displays two emission peaks in the innermost region of the circumstellar dust shell at the three wavelengths observed. This two-peaked mid-infrared morphology is interpreted as an equatorial density enhancement revealing the presence of a dusty toroidal structure with a 0.4$''$ radius size (or $\sim$640 AU corresponding to a dynamical age of $\sim$190 yr at the assumed distance of 1.6 kpc). The observed size is used to derive the dust temperature at the inner radius of the shell. This result has been combined with the information derived from the ISO observations of I16594 to conclude that the mid-infrared emission detected in our TIMMI2

images must be dominated by PAH molecules or clusters which must be mainly distributed along the torus, as suggested by the similar size and morphology observed in all filters. We have also found that the axis of symmetry observed in the mid-infrared is well aligned with only one of the bipolar outflows (at P.A.∼84°) seen as optical reflection nebulae in the optical HST images. We suggest that the multiple outflow formation has not been coeval and that, at present, the outflow material is being ejected in this direction. Consistently, the H_2 shocked-emission seen in the HST NICMOS image is mainly distributed along the same bipolar axis where the fast post-AGB wind is interacting with the slow moving material ejected during the previous AGB phase. The presence of several other bipolar outflows at a variety of position angles may be the result of past episodic mass loss events.

I07027 exhibits a slightly asymmetric mid-IR emission core which is only marginally extended along the north-south direction with FWHM=0.3″ at 8.6 and 11.5 μm. This is the same orientation observed in recent HST images of the source taken in the near-infrared. The mid-infrared emission is attributed to a combination of emission from highly ionized, small PAH molecules plus relatively warm dust continuum located very close to the central star. The characteristics of the PAH emission observed in the ISO spectrum are also consistent with this interpretation. Taking into account the spatial distribution of the C-rich material deduced from our observations and because the OH maser emission from I07027 is expected to be located in the external and cooler regions, we propose that the dual chemistry observed in I07027 must be interpreted as the consequence of a recent thermal pulse (probably at the end of the previous AGB phase) which has switched the chemistry of the central star from the original O-rich composition to a C-rich one within the last 500 yrs. This might be the commom mechanism which originates the dual chemistry and strong stellar winds usually observed in other [WC]-type CSPNe.

REFERENCES

Allain, T., Leach, S., & Sedlmayr, E. 1996, A&A, 305, 616

Allamandola, L. J., Hudgins, D. M.,& Sandford, S. A. 1999, ApJL, 511, 115

Asplund, M., Lambert, D. L., Kipper, T., Pollacco, D., & Shetrone, M. D. 1999, A&A, 343, 507

Balick, B., & Frank, A. 2002, ARA&A, 40, 439

Beichman, C.A., Neugebauer, G., Habing, H.J., Clegg, P.E., Chester, T.J. 1988, (Washington, DC:GPO), NASA RP-1190, vol 1

Blöcker, T. 2001, Ap&SS, 275, 1

Bond, H.E. & Livio, M., 1990, ApJ 355, 568

Cardelli, J. A., Clayton, C., & Mathis, J. S. 1989, ApJ, 345, 245

Cohen, M., Barlow, M. J., Liu, X. -W., & Jones, A. F. 2002, MNRAS, 332, 879

Colangeli, L., Mennella, V., Palumbo, P., Rotundi, A., & Bussoletti, E. 1995, A&ASS, 113, 561

De Marco, O., & Soker, N. 2002, PASP, 114, 602

De Marco, O., Barlow, M. J., & Cohen, M. 2002, ApJ, 574, 83

Doublier, V., Billeres, M., Lo Curto, G., Weilenmann, U., Kaufl, U., Sterzick, M., & Hainaut, O. 2004, LSO-MAN-ESO-9XXXX-X/X.0, in preparation

Draine, B. T., & Lee, H. M. 1984, ApJ, 285, 89

Evans, N.J. 1980. IAU Symp. 87, "*Interstellar molecules*", Dordrecht, D. Reidel Publishing Co. p.1

García-Hernández, D. A., Manchado, A., García-Lario, P., Domínguez-Tagle, C., Conway, G. M., & Prada, F. 2002, A&A, 387, 955

García-Lario, P., Manchado, A., Pych, W., & Pottasch, S. R. 1997, A&AS, 126, 479

García-Lario, P., Manchado, A., Ulla, A., & Manteiga, M. 1999, ApJ, 513, 941

García-Segura, G., Langer, N. & Rozyczka, M. 1999, ApJ, 517, 767

García-Segura, G., & López, J. A. 2000, ApJ, 544, 336

Guerrero, M. A., & Manchado, A. 1998, ApJ, 508, 262

Hajduk, M., Zijlstra, A. A., Herwig, F., van Hoof, P. A. M., Kerber, F., Kimeswenger, S., Pollacco, D. L., Evans, A., Lopéz, José A., Bryce, M., Eyres, S. P. S., & Matsuura, M. 2005, Science, 308, 231

Herwig, F., Blöcker, T., Schönberner, D., & El Eid, M. 1997, A&A, 324, L81

Herwig, F., Blöcker, T., Langer, N., & Driebe, T. 1999, A&A, 349, 5

Herwig, F. 2000, A&A, 360, 952

Herwig, F. 2001, Ap&SS, 275, 15

Hony, S., Waters, L. B. F. M., & Tielens, A. G. G. M. 2002, A&A, 390, 533

Hrivnak, B. J., Kwok, S., & Su, K. Y. L. 1999, ApJ, 542, 849

Hrivnak, B. J., Volk, K., & Kwok, S. 1999, BAAS, 31, 1536

Hrivnak, B. J., Volk, K., & Kwok, S. 2000, ApJ, 535, 275

Hrivnak, B.J., Kelly, D.M., & Su, Y.L. 2004, in "*Asymmetrical Planetary Nebulae III: Winds, Structure and the Thunderbird*", eds. M. Meixner, J.H. Kastner, B. Balick and N. Soker. ASP Conference Proceedings, Vol. 313, p.175

Jura, M., Balm, S. P., & Kahane, C. 1995,ApJ, 453, 721

Jura, M., Chen, C., & Plavchan, P. 2002, ApJ, 569, 964

Justtanont, K., Barlow, M. J., Skinner, C. J., Roche, P. F., Aitken, D. K., & Smith, C. H. 1996, A&A, 309, 612

Käufl, H.-U., Sterzik, M. F., Siebenmorgen, R., Weilenmann, U., Relke, H., Hron, J., & Sperl, M. 2003, SPIE 4841, 117

Koike, C., Hasegawa, H., & Manabe, A. 1980, Ap&SS, 67, 495

Kwok, S., Purton, C. R., & Fitzgerald, P. M. 1978, ApJL, 219, 125

Kwok, S. 1993, IAU Symp. 155, "*Planetary Nebulae*", eds. Edited by R. Weinberger and A. Acker. Kluwer Academic Publishers; Dordrecht, p.263

Kwok, S., Hrivnak, B. J., & Geballe, T. R. 1995, ApJ, 454, 394

Lechner, M. F. M., & Kimeswenger, S. 2004, A&A, 426, 145

Leuenhagen, U., & Hamann, W. -R. 1998, 330, 265

Loup, C., Forveille, T., Nyman, L. A., & Omont, A. 1990, A&A, 227, L29

Manchado, A., Villaver, E., Stanghellini, L. & Guerrero, M. A., 2000, in *"Asymmetrical Planetary Nebulae II: From Origins to Microstructures"*, eds. J.H. Kastner, N. Soker, and S. Rappaport. ASP Conference Series, Vol. 199, p. 17

Matsuura, M., Zijlstra, A. A., Molster, F. J., Hony, S., Waters, L. B. F. M., Kemper, F., Bowey, J. E., Chihara, H., Koike, C., & Keller, L. P. 2004, ApJ, 604, 791

Meixner, M., Skinner, C. J., Graham, J. R., Keto, E., Jernigan, J. G., & Arens, J. F. 1997, ApJ, 482, 897

Meixner, M., Ueta, T., Dayal, A., Hora, J. L., Fazio, G. Hrivnak, B. J., Skinner, C. J., Hoffmann, W. F., & Deutsch, L. K. 1999, ApJS, 122, 221

Mellema, G. 1993, Ph D. Thesis, Sterrewacht Leiden

Menzies, J. W., & Wolstencroft, R. D. 1990, MNRAS, 247, 177

Molster, F. J., Waters, L. B. F. M., Tielens, A. G. G. M., & Barlow, M. J. 2002a, A&A, 382, 184

Molster, F. J., Waters, L. B. F. M., Tielens, A. G. G. M., Koike, C. & Chihara, H. 2002b, A&A, 382, 241

Morris, M. 1987, PASP 99, 115

Myers, P. C., Fuller, Gary A., Mathieu, R. D., Beichman, C. A., Benson, P. J., Schild, R. E., & Emerson, J. P. 1987, ApJ, 319, 340 Neugebauer, G. et al. 1986, A&AS, 65, 607

Pascoli, G. 1992, PASP, 104, 350

Pauzat, F., Talbit, D., & Ellinger, Y. 1997, A&A, 319, 318

Peeters, E., Hony, S., Van Kerckhoven, C., Tielens, A. G. G. M., Allamandola, L. J., Hudgins, D. M., & Bauschlicher, C. W. 2002, A&A, 390, 1089

Reimann, H. -G., Linz, H., Wagner, R., Relke, H., Käufl, H. -U., Dietzsch, E., Sperl, M., & Hron, J. 2000, SPIE 4008, 1132

Riera, A., García-Lario, P., Manchado, A., Bobrowsky, M., & Estalella, R. 2003, A&A, 401, 1039

Schönberner, D. 1987, in *"Late stages of stellar evolution"*, Dordrecht, D. Reidel. Publishing Co, p. 337

Scoville, N. Z., & Kwan, J. 1976, ApJ, 206, 718

Soker, N. & Harpar, A., 1992, PASP, 104, 923

Speck, A.K. & Hofmeister, A.M. 2003, IAU Symp. 209, "*Planetary Nebulae: Their Evolution and Role in the Universe*", eds. S. Kwok, M. Dopita and R. Sutherland. ASP, p.315

Stasynska, G., Gorny, S.K., Tylenda, R. 1997, A&A 327, 736

Su, K. Y. L., Hrivnak, B. J., Kwok, S., & Sahai, R. 2003, AJ, 126, 848

Surendiranath, R. 2002. A&A, 390, 667

te Lintel Hekkert, P., Caswell, J. L., Habing, H. J., Haynes, & R. F., Norris, R. P. 1991, A&AS, 90, 327

Ueta, T., Meixner, M., & Bobrowsky, M. 2000. ApJ, 528, 861

Ueta, T., Meixner, M., Hinz, P. M., Hoffmann, W. F., Brandner, W., Dayal, A., Deutsch, L. K., Fazio, G. G., & Hora, J. L. 2001, ApJ, 557, 831

Ueta, T., & Meixner, M. 2003, ApJ, 586, 1338

Ueta, T., Murakawa, K., & Meixner, M. 2005, AJ, 129, 1625

Van de Steene, G. C., & Pottasch, S. R. 1993, A&A, 274, 895

Van de Steene, G. C., & van Hoof, P. A. M. 2003, A&A, 406, 773

Van de Steene, G. C., van Hoof, P. A. M., & Wood, P. R. 2000, A&A, 362, 984

Van de Steene, G.C., Wood, P.R. & van Hoof, P.A.M. 2000, in "*Asymmetrical Planetary Nebulae II: From Origins to Microstructures*", eds. J.H. Kastner, N. Soker, and S. Rappaport. ASP Conference Series, Vol. 199, p. 191

van der Veen, W. E. C. J., Habing, H. J., & Geballe, T. R. 1989, A&A, 226, 108

Van Winckel, H. 2003, ARA&A, 41, 391

von Helden, G., Tielens, A. G. G. M., van Heijnsbergen, D., Duncan, M. A., Hony, S., Waters, L. B. F. M., & Meijer, G. 2000, Sci, 288, 313

Volk, K. M., & Kwok, S. 1989, ApJ, 342, 345

Waters, L. B. F. M., Cami, J., de Jong, T., Molster, F. J., van Loon, J. Th., Bouwman, J., de Koter, A., Waelkens, C., Van Winckel, H., & Morris, P. W. 1998, Nature, 391, 868

Yamamura, I., Dominik, C., de Jong, T., Waters, L. B. F. M., & Molster, F. J. 2000, A&A, 363, 629

Zijlstra, A. A., Te Lintel Hekkert, P., Pottasch, S. R., Caswell, J. L., Ratag, M., & Habing, H. J. 1989, A&A, 217, 157

Zijlstra, A. A., Gaylard, M. J., te Lintel Hekkert, P., Menzies, J., Nyman, L.-A., & Schwarz, H. E. 1991, A&A, 243, L9

Zijlstra, A. A. 2001, Ap&SS, 275, 79

Table 1.   Summary of the ESO 3.6m/TIMMI2 Mid-Infrared Observations.

Object	Date	Filter	$\lambda_c(\Delta\lambda)$ (μm)	T_{Total} (s)	Size[a] (arcsec)	PSF Size[b] (arcsec)	Flux[c] (Jy)	Peak (Jy arcsec^{-2})
IRAS 16594−4656	2001 Oct 9	N1	8.6(1.67)	120.4	∼1.7 x 1.6	0.57	14	5
. . .	. . .	N11.9	11.5(1.89)	107.5	∼1.8 × 1.6	0.73	40	13
. . .	. . .	SiC	11.7(3.21)	161.3	∼1.8 × 1.6	0.75	35	11
IRAS 07027−7934	2001 Oct 10	N1	8.6(1.67)	120.4	0.65	0.57	19	23
. . .	. . .	N11.9	11.5(1.89)	107.5	0.83	0.73	19	17

[a]Major and minor axis length at 40% of the peak intensity or FWHM in the case of IRAS 07027−7934

[b]FWHM of the mean PSF adopted

[c]The fluxes are not color corrected

Table 2.   Mid-infrared Toroidal PPN/PNe sample.

IRAS Name	Torus[a]	Ref.[b]	Sp.Type[c]	Chem.[d]	Type[e]	Morph.[f]	PAHs[g]	21 μm[h]	Ref.[i]
07134+1005	R	1	F5 Iab	C	PPN	S+B	y	y	1
16594−4656	R	2	B7	C	PPN	S+M	y	y	2
17436+5003	R	3	F3 Ib	O	PPN	S+B	n	n	3
19114+0002	R*	4	G5 Ia	O	PPN/SG	S+M	n	n	3
21282+5050	R	1	O9	C	Young PN	S+B	y	n	4
22223+4327	U	4	G0 Ia	C	PPN	S+M	y	y	5
22272+5435	R	5	G5	C	PPN	S+M	y	y	6

[a]R: Two emission peaks clearly resolved. R*: The torus orientation is almost pole-on and it is seen as a ring. U: The two emission peaks are not resolved but there are evidences for the presence of a toroidal structure.

[b]References for the mid-infrared images and their classification: 1) Meixner et al. (1997); 2) This work; 3) Ueta, Meixner & Bobrowsky (2000); 4) Meixner et al. (1999); 5) Ueta et al. (2001).

[c]Spectral types taken from SIMBAD.

[d]C: C-rich. O: O-rich.

[e]Evolutionary classification.

[f]S+B: Star + bipolar. S+M: Star + multipolar. Optical morphology taken from Meixner et al. (1999). For IRAS 22223+4327 and IRAS 16594−4656 the HST images were retrieved from the HST Data Archive.

[g]Presence of the dust features at 3.3, 6.2, 7.7, 8.6 and 11.3 μm generally attributed to PAHs.

[h]Presence of the unidentified dust emission feature at 21 μm.

[i]References for the mid-infrared spectra: 1) Hrivnak, Volk & Kwok (2000); 2) García-Lario et al. (1999); 3) Molster et al. (2002a); 4) Justtanont et al. (1996); 5) Kwok, Hrivnak & Geballe (1995); 6) Hrivnak, Volk & Kwok (1999).
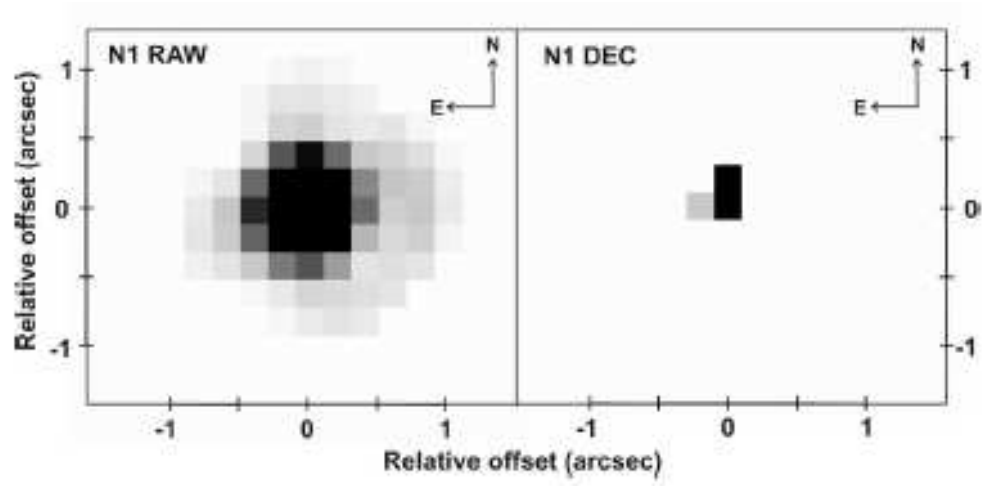
Fig. 1.— Illustrative example of the deconvolution of one of the observed standard stars showing the goodness of the deconvolution process. Raw mid-infrared image in the N1 (8.6 μm) filter (left) and the corresponding deconvolved image using the Lucy-Richardson algorithm (right).

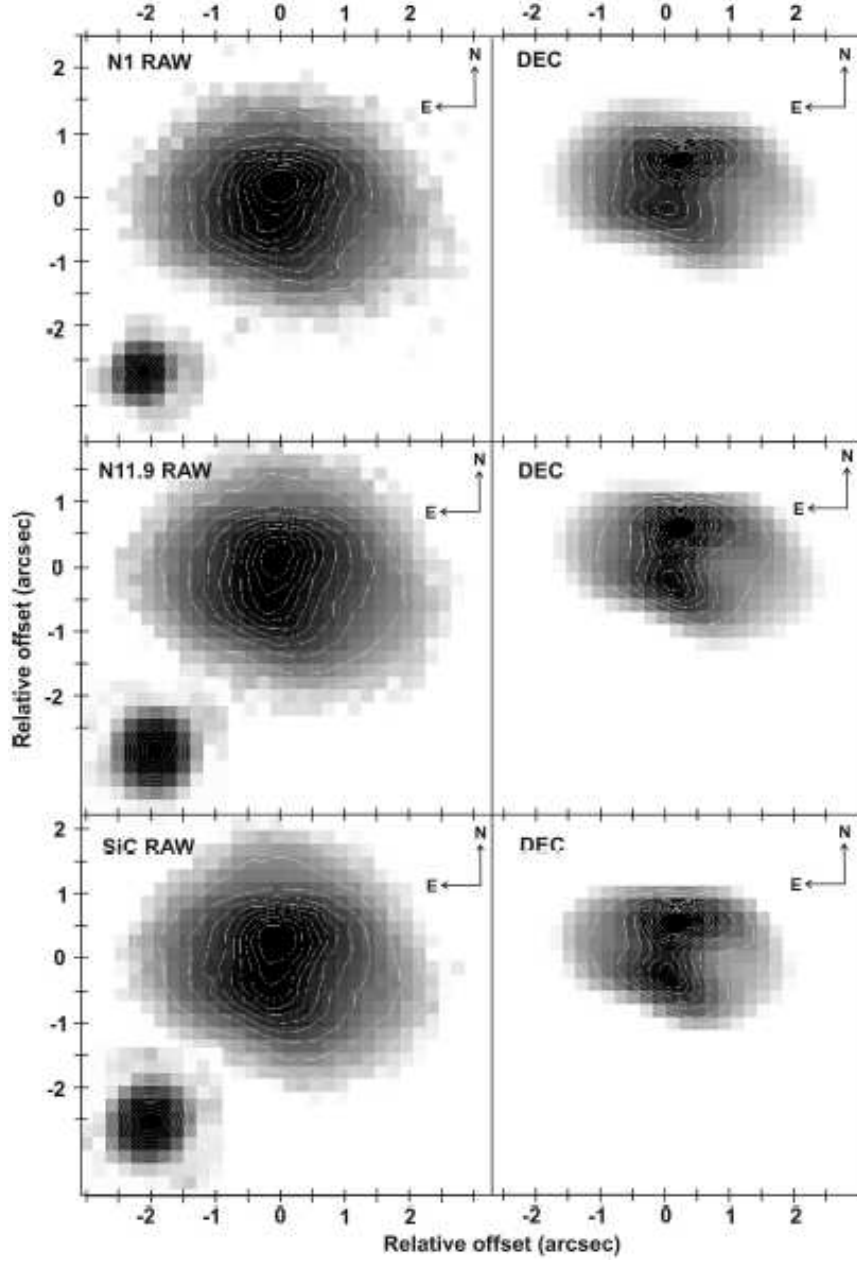Fig. 2.— From top to bottom, raw mid-infrared images of IRAS 16594−4656 in the N1 (8.6 μm), N11.9 (11.5 μm) and SiC (11.7 μm) filters (left) and the corresponding deconvolved images using the Lucy-Richardson algorithm (right). The tick marks show relative offsets from the center of the nebula in arcseconds. Contours range from 10% to 90% of the peak intensity (in steps of 10%) plus the outermost contour, which corresponds to 5% of the peak intensity (or $\sim$60 mJy at 10-σ level above the sky background). The insets show the standard star PSFs in each filter.
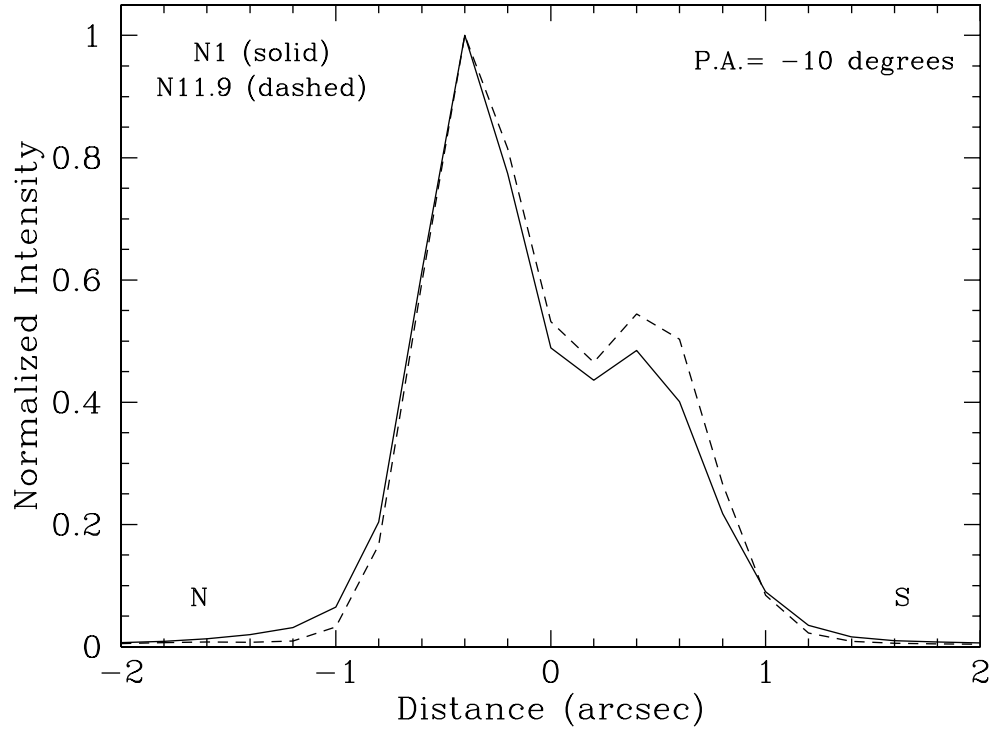
Fig. 3.— Normalized surface intensity profiles along the dust torus direction (from north to south) in IRAS 16594−4656. The solid and dashed lines correspond to the N1 (8.6 μm) and N11.9 (11.5 μm) filters, respectively. The center of the nebula (tentatively identified as the central star position, see text) corresponds to distance 0.
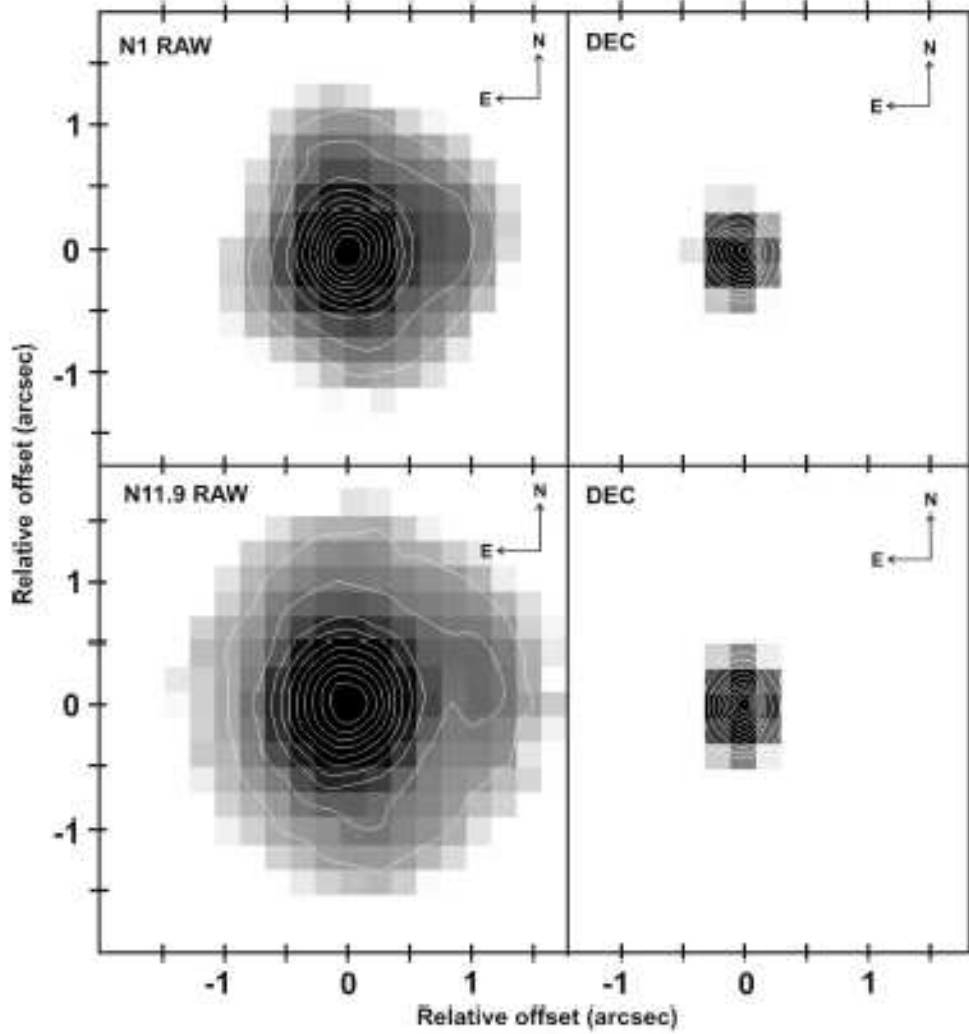
Fig. 4.— From top to bottom, raw mid-infrared images of IRAS 07027−7934 in the N1 (8.6 μm), and N11.9 (11.5 μm) filters (left) and the corresponding deconvolved images using the Lucy-Richardson algorithm (right). The tick marks show relative offsets from the center of the nebula in arcseconds. Contours range from 10% to 90% of the peak intensity (in steps of 10%) plus the outermost contour, which corresponds to 5% of the peak intensity (or $\sim$50 mJy at 7-σ level above the sky background).
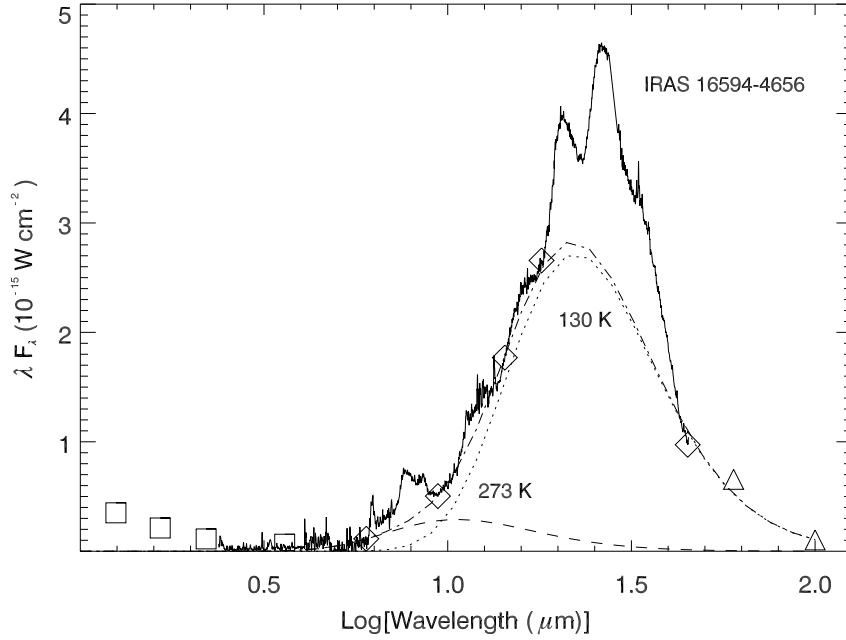
Fig. 5.— Two blackbody fitting of the SED of IRAS 16594−4656. The square symbols correspond to the dereddened JHKL photometry while the continuum points at 6, 9.4, 14.3, 18, and 45 μm that were carefully selected for the fitting from the SWS ISO spectrum correspond to the diamond symbols. The IRAS photometry at 60 and 100 μm are represented with triangle symbols. The best fit (dotted and dashed line) is obtained with the combination of two blackbodies with temperatures of 273 K (dashed line) and 130 K (dotted line), respectively. Note that the huge excess emission between 18−45 μm is mainly due to the presence of the strong 21 μm feature, the 26 μm feature and the broad 30 μm feature (see text).
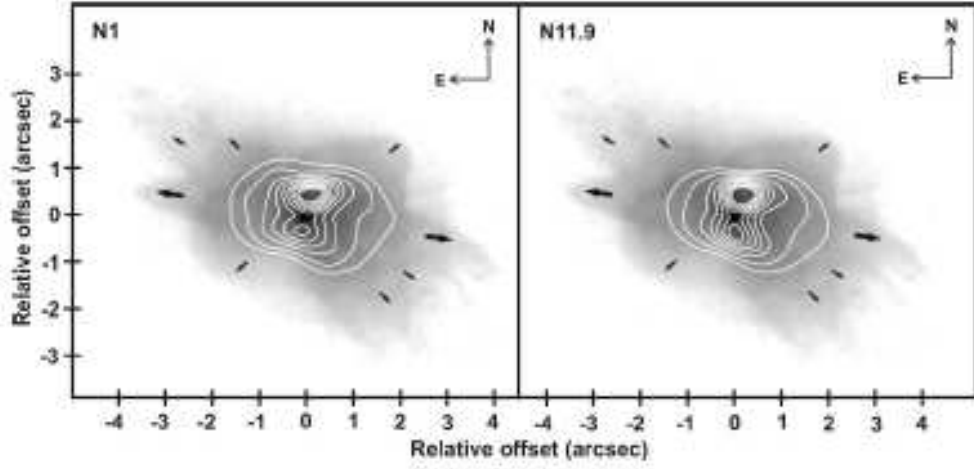
Fig. 6.— Contour maps of the deconvolved mid-infrared images taken in the N1 (8.6 μm) and N11.9 (11.5 μm) filters overlaid on the optical HST image of IRAS 16594−4656 in the F606W filter (taken from the HST Data Archive). The tick marks show relative offsets from the center of the nebula in arcseconds. The arrows indicate the direction of the various bipolar lobes identified in the optical images. The big one marks the lobe whose orientation is remarkably coincident with the mid-infrared axis defined by the dust torus.
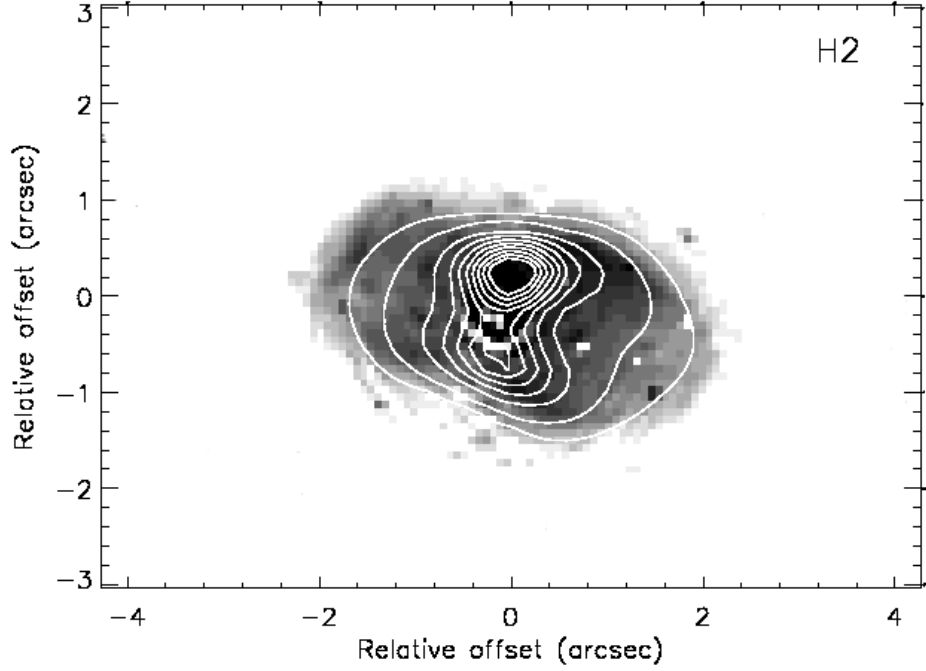
Fig. 7.— Contour map of the deconvolved mid-infrared image taken in the N11.9 (11.5 μm) filter overlaid on the HST-NICMOS image (taken from the HST Data Archive) showing the near-infrared H_2 emission at 2.122 μm detected in IRAS 16594−4656. The orientation is the same as in the other figures of the paper (north is up and east to the left) and the H_2 image is displayed on logarithmic-scale. Remarkably, the H_2 emission which nicely coincides with the mid-infrared emission is mainly distributed along the walls of the lobe at P.A.∼84° identified in the optical images of IRAS 16594−4656 (see Fig. 6). Note that the H_2 image was continuum-subtracted using the HST-NICMOS image containing the emission in the adjacent continuum at 2.15 μm.
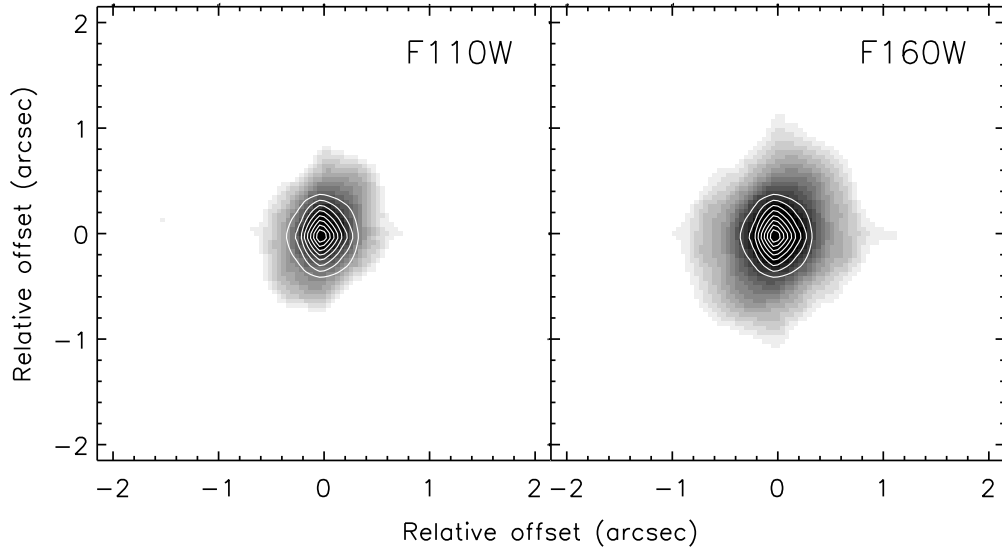
Fig. 8.— Contour map of the deconvolved mid-infrared image taken in the N11.9 (11.5 μm) filter overlaid on the logarithmic-scale near-infrared HST-NICMOS images of IRAS 07027−7934 (taken from the HST Data Archive) in the F110W (left panel) and F160W filters (right panel). Again, north is up and east to the left. Note that the near-infrared images show that indeed the inner regions have an elongated shape along the north-south direction, coincident with the orientation observed in our mid-infrared images (see text for more details).